

Polarisation-selective hotspots in metallic ring stack arrays

Laura J. Brooks,^{*} Jan Mertens, Richard W. Bowman, Rohit Chikkaraddy, Alan Sanders, and Jeremy J. Baumberg

NanoPhotonics Centre, Cavendish Laboratory, Department of Physics, University of Cambridge, JJ Thomson Avenue, Cambridge, CB3 0HE, UK
**ljb86@cam.ac.uk*

Abstract: We demonstrate a simple, scalable fabrication method for producing large-area arrays of vertically stacked metallic micro-rings, embedded in a deformable polymer sheet. Unusual polarisation-dependent hotspots are found to dominate the reflection images. To understand their origin, the arrays are characterized using point-scanning optical spectroscopy and directly compared to numerical simulations. Individual ring stacks act as microlenses, while polarisation-dependent hotspots arise at the connections between neighbouring stacks, which are comprised of parabolically-arranged parallel gold nanowires. The elastomeric properties of the polymer host opens the door to active control of the optics of this photonic material, through dynamic tuning of the nanowire spacings and array geometry.

Published by The Optical Society under the terms of the [Creative Commons Attribution 4.0 License](#). Further distribution of this work must maintain attribution to the author(s) and the published article's title, journal citation, and DOI.

OCIS codes: (050.1950) Diffraction gratings; (050.6875) Three-dimensional fabrication; (110.4234) Multispectral and hyperspectral imaging; (110.5220) Photolithography; (130.5440) Polarization-selective devices; (220.4000) Microstructure fabrication; (350.4238) Nanophotonics and photonic crystals.

References and links

1. H. K. Raut, V. A. Ganesh, A. S. Nair, and S. Ramakrishna, "Anti-reflective coatings: a critical, in-depth review," *Energy Environ. Sci.* **4**(10), 3779 (2011).
2. Y.-C. Chao, C.-Y. Chen, C.-A. Lin, and J.-H. He, "Light scattering by nanostructured anti-reflection coatings," *Energy Environ. Sci.* **4**(9), 3436 (2011).
3. E. E. Perl, C. T. Lin, W. E. McMahon, D. J. Friedman, and J. E. Bowers, "Ultrabroadband and wide-angle hybrid antireflection coatings with nanostructures," *IEEE J. Photovoltaics* **4**(3), 962–967 (2014).
4. Y. Yu, L. Wen, S. Song, and Q. Chen, "Transmissive/reflective structural color filters: theory and applications," *J. Nanomater.* **2014**(8), 1–17 (2014).
5. F. Cheng, J. Gao, T. S. Luk, and X. Yang, "Structural color printing based on plasmonic metasurfaces of perfect light absorption," *Sci. Rep.* **5**, 11045 (2015).
6. A. Saito, "Material design and structural color inspired by biomimetic approach," *Sci. Technol. Adv. Mater.* **12**(6), 064709 (2011).
7. S. J. Tan, L. Zhang, D. Zhu, X. M. Goh, Y. M. Wang, K. Kumar, C. W. Qiu, and J. K. W. Yang, "Plasmonic color palettes for photorealistic printing with aluminum nanostructures," *Nano Lett.* **14**(7), 4023–4029 (2014).
8. Y. K. Wu, A. E. Hollowell, C. Zhang, and L. J. Guo, "Angle-insensitive structural colours based on metallic nanocavities and coloured pixels beyond the diffraction limit," *Sci. Rep.* **3**, 1194 (2013).
9. X. Zhang, S. Ye, X. Zhang, Z. Li, S. Wu, J. Zhang, T. Wang, and B. Yang, "Panchromatic plasmonic color patterns: from embedded Ag nanohole arrays to elevated Ag nanohole arrays," *J. Mater. Chem. C Mater. Opt. Electron. Devices* **1**(5), 933–940 (2013).
10. Y. Zhao, Z. Xie, H. Gu, C. Zhu, and Z. Gu, "Bio-inspired variable structural color materials," *Chem. Soc. Rev.* **41**(8), 3297–3317 (2012).
11. N. Meinzer, W. L. Barnes, and I. R. Hooper, "Plasmonic meta-atoms and metasurfaces," *Nat. Photonics* **8**(12), 889–898 (2014).
12. N. Yu and F. Capasso, "Flat optics with designer metasurfaces," *Nat. Mater.* **13**(2), 139–150 (2014).
13. J. J. Cowan, "Holographic honeycomb microlens," *Opt. Eng.* **24**(5), 245796 (1985).
14. J. H. Yun, E. Lee, H. H. Park, D. W. Kim, W. A. Anderson, J. Kim, N. M. Litchinitser, J. Zeng, J. Yi, M. M. Kumar, and J. Sun, "Incident light adjustable solar cell by periodic nanolens architecture," *Sci. Rep.* **4**, 6879 (2014).

15. J. F. Betz, W. W. Yu, Y. Cheng, I. M. White, and G. W. Rubloff, "Simple SERS substrates: powerful, portable, and full of potential," *Phys. Chem. Chem. Phys.* **16**(6), 2224–2239 (2014).
16. J. W. Kemling, A. J. Qavi, R. C. Bailey, and K. S. Suslick, "Nanostructured substrates for optical sensing," *J. Phys. Chem. Lett.* **2**(22), 2934–2944 (2011).
17. S. Aksu, M. Huang, A. Artar, A. A. Yanik, S. Selvarasah, M. R. Dokmeci, and H. Altug, "Flexible plasmonics on unconventional and nonplanar substrates," *Adv. Mater.* **23**(38), 4422–4430 (2011).
18. L. Zhu, J. Kapraun, J. Ferrara, and C. J. Chang-Hasnain, "Flexible photonic metastructures for tunable coloration," *Optica* **2**(3), 255–258 (2015).
19. K. Du, I. Wathuthanthri, Y. Liu, W. Xu, and C.-H. Choi, "Wafer-scale pattern transfer of metal nanostructures on polydimethylsiloxane (PDMS) substrates via holographic nanopatterns," *ACS Appl. Mater. Interfaces* **4**(10), 5505–5514 (2012).
20. M. Kolle, B. Zheng, N. Gibbons, J. J. Baumberg, and U. Steiner, "Stretch-tuneable dielectric mirrors and optical microcavities," *Opt. Express* **18**(5), 4356–4364 (2010).
21. M. G. Millyard, F. Huang, R. White, E. Spigone, J. Kivioja, and J. J. Baumberg, "Stretch-induced plasmonic anisotropy of self-assembled gold nanoparticle mats," *Appl. Phys. Lett.* **100**(7), 073101 (2012).
22. Q. Zhao, A. Haines, D. Snoswell, C. Keplinger, R. Kaltseis, S. Bauer, I. Graz, R. Denk, P. Spahn, G. Hellmann, and J. J. Baumberg, "Electric-field-tuned color in photonic crystal elastomers," *Appl. Phys. Lett.* **100**(10), 101902 (2012).
23. S. Walia, C. M. Shah, P. Gutruf, H. Nili, D. R. Chowdhury, W. Withayachumnankul, M. Bhaskaran, and S. Sriram, "Flexible metasurfaces and metamaterials: A review of materials and fabrication processes at micro- and nano-scales," *Appl. Phys. Rev.* **2**(1), 011303 (2015).
24. A. Di Falco, M. Ploschner, and T. F. Krauss, "Flexible metamaterials at visible wavelengths," *New J. Phys.* **12**(11), 113006 (2010).
25. L. Gao, Y. Zhang, H. Zhang, S. Doshay, X. Xie, H. Luo, D. Shah, Y. Shi, S. Xu, H. Fang, J. A. Fan, P. Nordlander, Y. Huang, and J. A. Rogers, "Optics and nonlinear buckling mechanics in large-area, highly stretchable arrays of plasmonic nanostructures," *ACS Nano* **9**(6), 5968–5975 (2015).
26. M. Maldovan and E. L. Thomas, *Periodic Materials and Interference Lithography: For Photonics, Phononics and Mechanics* (Wiley-VCH, 2009).
27. E. Ertorer, F. Vasefi, J. Keshwah, M. Najiminaini, C. Halfpap, U. Langbein, J. J. L. Carson, D. W. Hamilton, and S. Mittler, "Large area periodic, systematically changing, multishape nanostructures by laser interference lithography and cell response to these topographies," *J. Biomed. Opt.* **18**(3), 035002 (2013).
28. R. J. Moerland, J. E. Koskela, A. Kravchenko, M. Simberg, S. van der Vegte, M. Kaivola, A. Priimagi, and R. H. A. Ras, "Large-area arrays of three-dimensional plasmonic subwavelength-sized structures from azopolymer surface-relief gratings," *Mater. Horiz.* **1**(1), 74–80 (2014).
29. A. J. Wolf, H. Hauser, V. Kübler, C. Walk, O. Höhn, and B. Bläsi, "Origination of nano- and microstructures on large areas by interference lithography," *Microelectron. Eng.* **98**, 293–296 (2012).
30. G. Si, Q. Wang, J. Lv, L. Miao, F. Wang, and S. Peng, "Interference lithography patterned large area plasmonic nanodisks for infrared detection," *Mater. Lett.* **128**, 373–375 (2014).
31. C. A. Mack, "Analytical expression for the standing wave intensity in photoresist," *Appl. Opt.* **25**(12), 1958 (1986).
32. G. Kostovski, A. Mitchell, A. Holland, and M. Austin, "Sidewall corrugation lithography: Bulk fabrication of ordered nanowires, nanoribbons, and nanorings," *Appl. Phys. Lett.* **92**(22), 223109 (2008).
33. L. J. Brooks, J. Mertens, R. W. Bowman, R. Chikkaraddy, A. Sanders, and J. J. Baumberg, Research data supporting "Polarisation-selective hotspots in metallic ring stack arrays," <https://www.repository.cam.ac.uk/handle/1810/253373>.
34. P.-K. Wei, H.-L. Chou, and Y.-C. Chen, "Subwavelength focusing in the near field in mesoscale air-dielectric structures," *Opt. Lett.* **29**(5), 433–435 (2004).

1. Introduction

The optical properties of a material can be drastically modified by texturing its surface on the micro or nano scale. Anti-reflection coatings [1–3], diffraction gratings, structural colour materials [4–10], metasurfaces [11,12], micro- and nanolens arrays [13,14], and sensing substrates [15,16] are just some of the examples in which surface structure generates optical functionality. Novel properties can also be engineered by combining two or more different materials into an artificial composite. In this context, elastomeric materials are of special interest, since they provide both the material conformability required for many emerging applications, and a mechanism for actively tuning the optical properties [17–25]. In this work, we develop metal-polymer composites with 3D surface relief, incorporating the mechanical flexibility of a deformable elastomer, with the desirable optical properties of a nanostructured metal. The resulting flexible photonic material comprises an array of vertically-stacked gold rings, embedded in a 3D nanostructured polydimethylsiloxane (PDMS) membrane. Light scattered by the metallic constituents, and its interaction with the sculpted surface, leads to the formation of polarisation-selective hotspots. The optical properties of the arrays are

investigated using microscopy and spectroscopy as well as numerical simulations, which together reveal the origin of the unusual polarization-selective properties.

While there is a high demand for flexible photonic materials for many devices, such as sensors, structural colour coatings, security features and display technologies, these applications require simple and fast fabrication methods to enable mass production on a large scale. In this paper, we demonstrate a scalable route, suitable for the manufacture of large-area sheets of such photonic materials.

2. Sample design and fabrication

To produce samples with 3D surface relief over a large area in a scalable way, we utilise laser interference lithography (LIL), a mask-free photolithographic technique in which fringe patterns generated by interfering laser beams are recorded directly into a photoresist [26]. Using this method, periodic features can be inscribed across the illuminated region using exposures of just a few seconds, making LIL a viable route for rapid industrial manufacture on a large scale [27–30]. As detailed below, this technique allows us to create arrays of 3D micron-high features with sub-100 nm intricate structure, that can be harnessed for photonics applications. We use gold coatings since the strong optical response of the plasmonic metal provides the maximum opportunity for effective local coupling of the optical fields.

The stacked gold ring arrays are fabricated in a three-step process, comprising: (1) preparation of ‘eggbox’ template structures in photoresist, (2) metal deposition onto the templates, and (3) transfer of the metallic arrays into the PDMS elastomer. The procedure is outlined in Fig. 1.

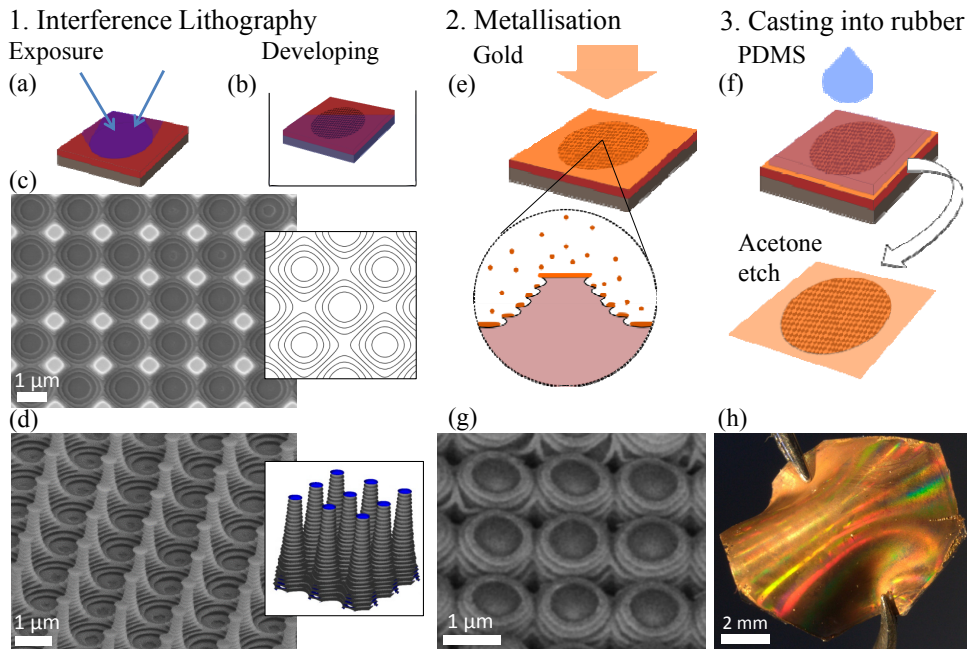


Fig. 1. Fabrication process. (a) Templates are patterned by 2-beam laser interference lithography, in a sequence of two orthogonal exposures (b) Exposed regions are dissolved in developer solution. (c) Top-view, and (d) side-view SEMs of the developed template structures, showing their ‘eggbox’ topography and sidewall corrugations. Insets show the total calculated intensity profile resulting from two crossed exposures. (e) Gold deposition onto corrugated templates forms the stacked metallic rings. (f) Casting into PDMS and etching of the photoresist produces a free-standing structured membrane embedded with gold rings. (g) Side-view SEM of the finished ring stack array. (h) Photograph of the flexible membrane, showing diffractive colouration under deformation.

2.1 Template structure preparation

In the first step, template structures are prepared using laser interference lithography. A 2 μm layer of resist (AZ 5214 E) is spin-coated onto polished silicon substrates, and patterned using a pair of ultra-violet (405 nm) laser beams. The beams, which are *s*-polarised and incident at an angle of 10° to the sample's surface normal, are brought to overlap at the plane of the substrate (Fig. 1(a)). In this configuration, a 1D-periodic fringe pattern is generated with a grating constant of 1.5 μm , however this periodicity can be tuned from 300 nm up to several microns, simply by varying the angle between the interfering beams. To produce a 2D-periodic array, a sequence of two exposures is employed, with a 90° rotation of the sample between illuminations. The resulting intensity pattern recorded into the resist is therefore the sum of the two exposures, plotted in the inset of Fig. 1(c). When the photoresist is developed (Fig. 1(b)), this produces a square array of 'posts' and 'cups', as shown in Fig. 1(d), with a topography reminiscent of an eggbox.

2.2 Gold deposition

The LIL eggbox structures feature highly corrugated sidewalls, as seen in Fig. 1(d), which are essential for templating the vertically stacked rings. Corrugations arise from reflection of the LIL beams from the surface of the flat silicon substrate. Interference between the incident and reflected laser beams creates a standing wave in the resist layer, modulating the intensity pattern in the vertical direction [31] to create sidewall 'ribs' with a periodicity of 120 nm. Considerable effort is usually given to suppressing the standing wave effect in photolithographic techniques. However, it has also been demonstrated that ribbed sidewalls can prove useful for templating vertically-stacked structures [32]. In this work, we utilise such corrugation-templating to produce a novel 3D photonic structure with intriguing optical properties. The ribbed eggbox templates are metallised with electron-beam deposition of a 65 nm layer of gold, at normal incidence, designed to ensure the stacked rings are not touching. As depicted in Fig. 1(e), gold atoms land on the upper surface of the sidewall ribs, forming discrete layers of well-defined gold rings that are arranged in a highly ordered, vertically-aligned stack.

2.3 Transfer to PDMS

In the last step, the ring stack array is transferred into the surface of a PDMS membrane. A 10:1 mixture of base and curing agent (Sylgard 184, Dow Corning) is drop-cast onto the metallised templates, as shown in Fig. 1(f), and cured at 70°C for 5 hours. Using acetone, the photoresist is dissolved from the membrane, releasing the PDMS from the Si substrate, and leaving the gold ring stacks embedded in the elastomer. The rings retain their vertical stacking in the surface of the polymer, creating a free-standing and deformable membrane, textured with an inverted eggbox lattice of stacked gold rings (Figs. 1(g) and 1(h)).

Scanning electron micrographs (SEMs) of both the metallised template and its resulting ring stack array, are shown in Fig. 2. The inverted impressions of the eggbox template 'posts', form square wells in the PDMS membrane, while the 'cups' of the eggbox produce an array of domed protrusions in the elastomer. The outer surface of each dome is stratified into layers of 65nm-thick gold rings. A side-view SEM of the ring stacks in Fig. 2(c) illustrates the vertical layering of the structure. The ring diameter increases with increasing depth into the membrane, and by the third layer from the surface, rings merge laterally into a connected mesh. Each ring stack is therefore joined to its neighbours on each side across the interconnections marked with yellow outlines in Fig. 2.

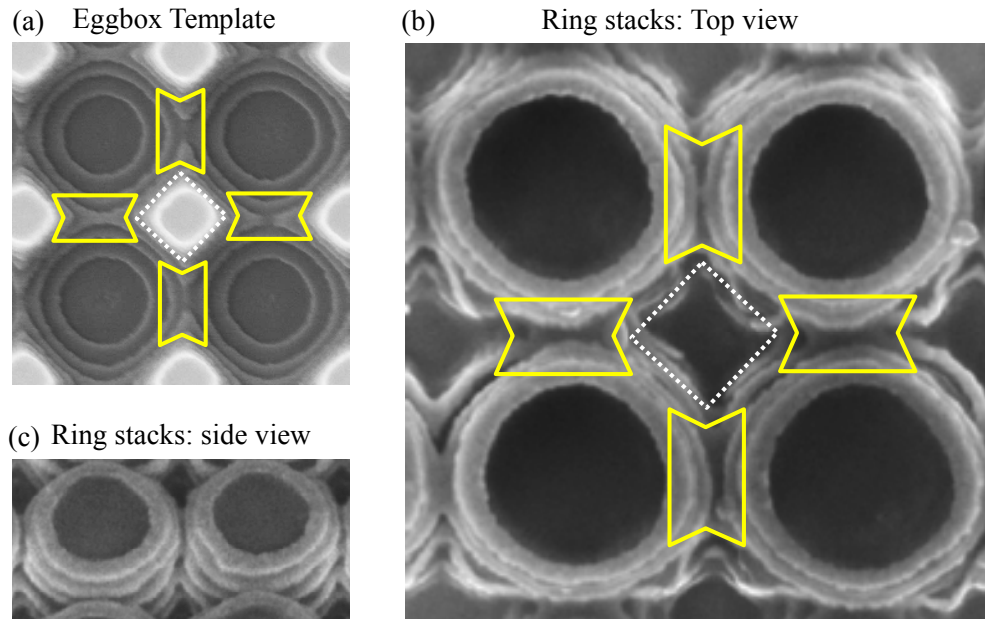


Fig. 2. Sample morphology. (a) Top-view SEM of the eggbox template structure in photoresist. One unit cell is $1.5 \times 1.5 \mu\text{m}$. (b) Top-view SEM of the finished ring stack array in PDMS. White dashed lines indicate the posts of the eggbox template, which produce square wells between the ring stacks. Yellow solid lines mark the interconnections between neighbouring stacks. (c) Side-view SEM of the ring stacks.

3. Optical properties

3.1 Polarisation-selective hotspots

The gold-PDMS composites are iridescent due to diffraction from the grating-like surface, and appear brightly coloured when the sample is deformed or viewed at an angle, as seen in Fig. 1(h). At normal incidence the material appears gold to the unaided eye, however bright-field optical microscope images (Figs. 3(b) and 3(c)) reveal that the microscale surface features are strongly coloured. The ring stacks appear green, while intense red spots are observed at the connecting points between adjacent stacks. These ‘hotspots’ are polarisation-sensitive, occurring only when the incident light is polarised orthogonally to the line connecting the stacks. An optical microscope image, with light polarised along the x -direction, is shown in Fig. 3(b). In this case, it is the set of connections linking the rings along y which appear red, while the connections directed along x are dark. Conversely in Fig. 3(c), in which incident light is y -polarised, it is the hotspots along the x -direction that are activated. It is therefore possible to selectively activate a set of hotspots either along x or along y , simply by switching the linear polarisation of the incident field.

3.2 Optical characterization

To understand the origin of these effects, the optical response of the structure is measured by polarisation-resolved point-scanning spectroscopy in a custom microscope. Samples are mounted on a translation stage with fine piezo control, and confocally illuminated in dark field configuration with a tightly-focussed white-light laser spot. A broadband polarising beamsplitter cube is used to separate each linear polarisation component of the collected light. Samples are hyperspectrally measured by scanning in along the x - and y -directions with steps of 50 nm, recording the scattered light spectrum at each spatial location. The scanned region of the sample spans several unit cells which are averaged together to produce a single low-

noise data set. The mirror symmetry along the x and y axes was also exploited to average together the four quadrants of the unit cell.

The spectral response at the hotspot locations is plotted in Fig. 4(b). When the hotspots are activated, the scattering spectrum is dominated by a peak at 660 nm, consistent with their strong red appearance in the microscope images. Meanwhile, the signals from the inactive hotspots in the orthogonal orientation are weak.

Intensity maps of the averaged unit cell, sliced at the peak hotspot wavelength of 660 nm, reconstruct the images seen directly in the microscope (Fig. 4(a)). For clarity the data is tiled into a 2×2 array, displaying four connected ring stacks. The map confirms that the hotspots are located at the connection points between the stacks, and that the intense red scattering is seen only when light is polarised *tangentially* to the rings at the connection (indicated by solid yellow lines in Fig. 4(a)), while connections in the other direction of polarisation (white dashed lines) are dark.

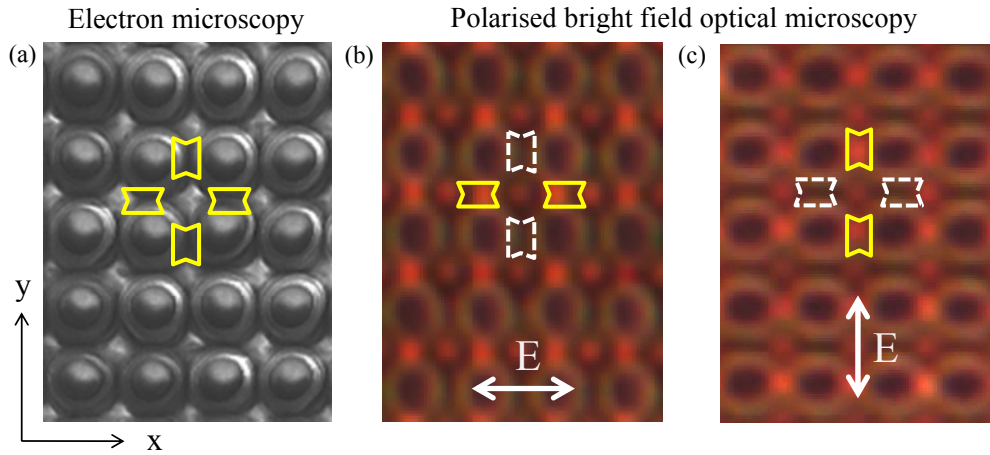


Fig. 3. Polarisation-selective hotspots. (a) Top-view SEM of a typical sample region. Yellow outlines indicate connecting points between ring stacks. (b, c) Bright field optical microscope images of another sample region, illuminated with light polarised along x and y , respectively. Ring stacks appear green, while the connecting bridges either scatter brightly in the red (yellow solid lines), or appear dark (white dashed lines), depending on the incident polarisation.

3.3 Numerical simulations

To numerically model the optical properties of the stacked ring arrays, a full 3D simulation of the unit cell is performed, using finite-difference time-domain (FDTD) calculations with periodic boundary conditions. The modelled structure, presented in Fig. 4(e), is constructed based on geometrical information from SEM images of the samples, together with calculations of the interference pattern used to create the template structures. To mimic the collection of light at different focal heights in the microscope, the FDTD results extracted from the model's monitor plane are numerically propagated in z , by applying a phase factor in Fourier space. For comparison with the experimental results, Fig. 4(c) shows the calculated field intensity in xy for a wavelength of 660 nm, with the z -plane chosen as the focal plane of the hotspots at this wavelength. The numerical simulations closely reproduce both the spatial position and the spectral response of the hotspots, as well as their polarisation-sensitivity. They confirm that active hotspots are characterised by a strong peak at 660 nm, in agreement with experimental observations. We attribute this scattering peak and its polarisation-dependence to antenna resonances excited by light polarised along the wire-like metallic connections, shown schematically in Fig. 5(a), and discussed below.

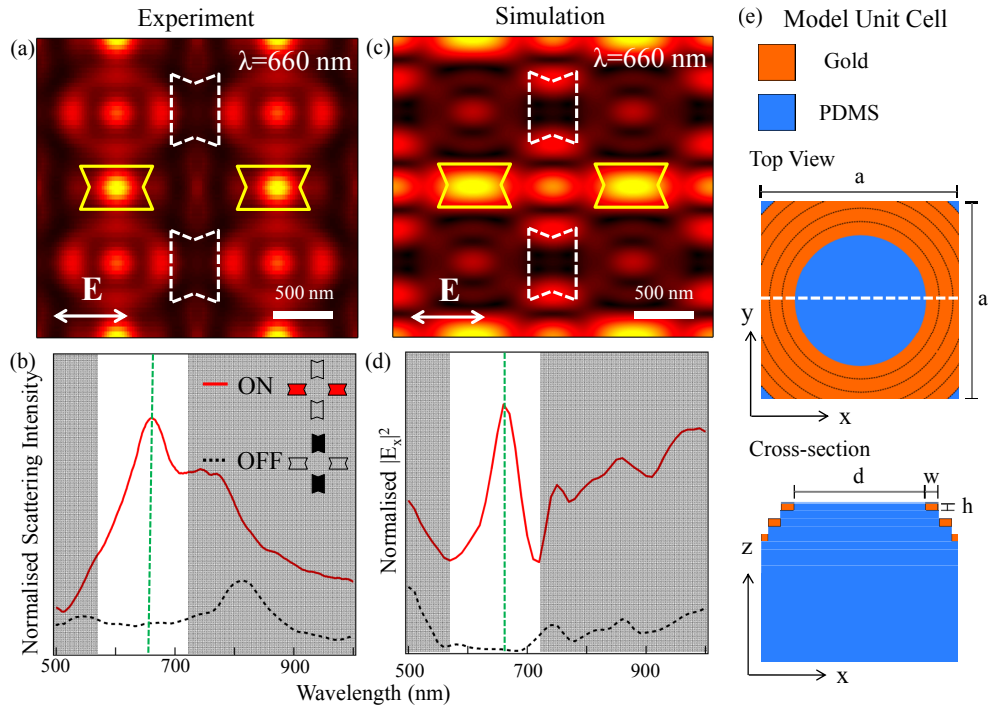


Fig. 4. Optical response of ring stack arrays, Dataset 1, Ref. [33]. (a) Average intensity map of a ring stack unit cell, tiled into a 2x2 array. The map is obtained by point-scanning spectroscopy with the optical field polarised along the x direction, sliced at a wavelength of 660 nm. Solid yellow lines indicate the active hotspots (ON configuration), while the hotspots in the OFF configuration are marked with a white dashed outline. (b) Scattering spectra of the hotspots in the ON (solid red trace) and OFF (dashed black trace) configurations. (c) Calculated intensity map at 660 nm in the focal plane of the sample, based on FDTD simulations. Solid yellow and dashed white lines mark the ON and OFF hotspots, respectively. (d) Calculated electric field intensity extracted at the hotspot locations for the ON (red) and OFF (black dashed) configurations. (e) Schematic of the modelled structure. White dashes in the top view indicate the line along which the xz cross-section is presented. The physical parameters of the model are set by the lattice constant $a = 1.5 \mu\text{m}$, the inner diameter of the uppermost ring $d = 1 \mu\text{m}$, the width of the rings $w = 100 \text{ nm}$, and the heights of the layers $h = 60 \text{ nm}$.

3.4 Focussing effects in ring stack arrays

Further insight into the formation of the hotspots is gained by considering the surface topography of the structure. Due to the wavelength-scale structuring of the surface, light scattered at different depths is strongly modulated by interference effects as it propagates, producing intricate patterns of the optical field that may be observed up to $8 \mu\text{m}$ above the membrane surface using white-light microscopy. These patterns are captured experimentally by scanning through the focus of the sample, recording images at a range of focal positions. The images, which each represent the optical field in xy in a given vertical plane, are stacked into a single data set reconstructing the field pattern in three dimensions. An xz slice through the 3D data set is shown in Fig. 5(c), cut through a line of ring stacks and active hotspots marked as a dashed white line in Fig. 5(b). Intense red spots are clearly observed, positioned directly above the membrane. The localisation of the spots is seen yet more clearly in Fig. 5(d), where the average xz optical field pattern is plotted for two unit cells. A white dashed oval indicates the hotspot location. In addition, a spectrally broader ‘green’ spot is also observed, located above the centre of the rings (green dashed oval). We attribute both these to

the focussing effect of the domed stacks, akin to microlensing phenomena reported in related structures [13,34].

The observed optical pattern in the xz plane is in excellent agreement with numerical simulations. The calculated xz slice at the hotspot peak wavelength of 660 nm, shown in Fig. 5(e), reproduces both the formation of focal spots above the stacks, and the polarisation-dependent hotspots in the V-shaped recesses between adjacent ring stacks.

The formation of hotspots within the interconnections is attributed to the V-shaped vertical arrangement of the radiating nanowire antennas, sketched in Fig. 5(a). This structure serves to concentrate the scattered light to an intense spot, much as a parabolic mirror produces a focus. The sub-micron focussing arrangement from the stack of parallel nanowires offers new possibilities for deformable optics, as the focal position depends on the the phase evolution of the light as it interacts with the ring structure, as well as the geometric arrangement of the nanowires that reradiate the light.

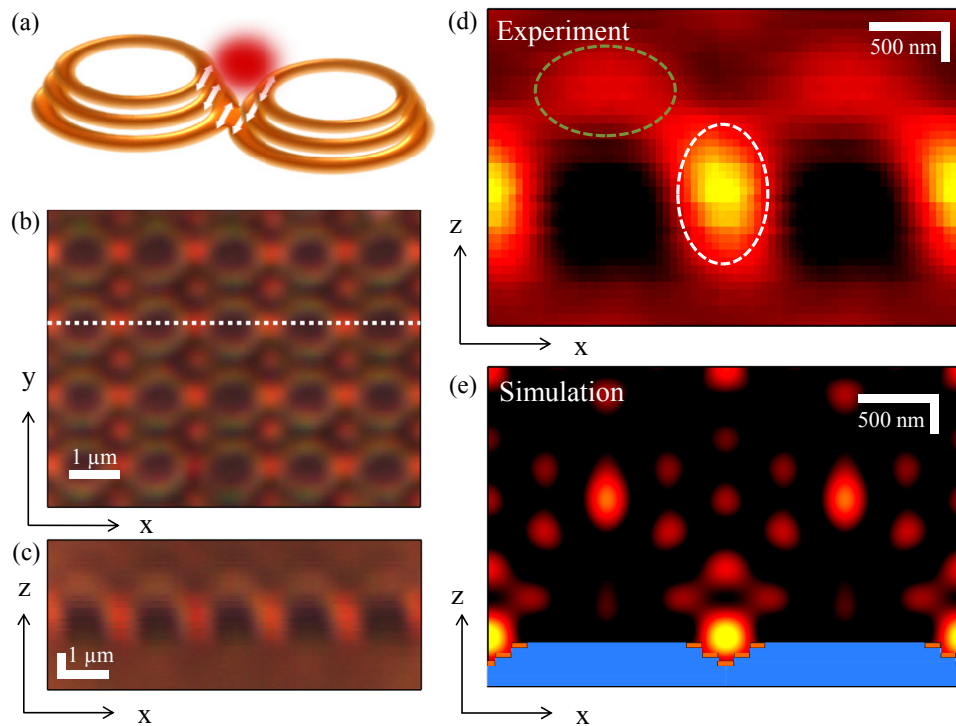


Fig. 5. Focussing effects, Dataset 1, Ref. [33]. (a) Schematic of the hotspot formation. Wire-like sections of the metallic rings at the interconnections support antenna resonances. Scattered light converges to focussed spots due to the geometrical arrangement of the wires. (b) Typical bright-field microscope image in the focal plane of the sample surface. White dashes indicate the line along which the xz section is plotted in (c). (d) An xz slice of the optical field for the red channel of the CCD detector. The data presents the average over several repeating units, and tiled to display two adjacent unit cells. A green dashed line indicates the position of the broadband focal spot above the ring stack, while a white dashed line marks the hotspot formed between the two stacks. (e) Calculated optical field at 660 nm in an xz slice equivalent to the experimental data. The blue/orange overlay shows the location of the physical PDMS/gold structure in the model.

4. Conclusion

In summary, we have developed a flexible photonic material with a novel microstructured surface, consisting of an array of metallic ring stacks in PDMS. The optical properties of the material were characterized by microscopy and point-scanning spectroscopy. Red hotspots are

observed in the focal plane of the surface, located in the recesses between the ring stacks, and can be switched on or off according to the polarisation of the incident optical field. This nanofocussing phenomenon arises from the antenna-like behavior of parallel metallic wires at the interconnections. Due to the V-shaped geometrical arrangement of the wires, re-radiated light converges to focused spots. This deformable elastomeric material can be employed as a conformable coating, while the simple, scalable fabrication route is well-suited for industrial production. Preliminary measurements show that it can be elastomerically deformed, opening the possibility to tunable surfaces, which are beyond the scope of the current paper. However, the use of LIL to create 3D intricate surface nanostructures for confining and manipulating light is clearly demonstrated, and shows robust performance over wide areas.

Acknowledgments

We are grateful for funding from the Cambridge NanoDTC, ERC LINASS 320503, and UK EPSRC grants EP/L027151/1 and EP/L015978/1. JM acknowledges support from the Winton Programme for the Physics of Sustainability, RWB thanks Queen's College Cambridge for financial support, and RC acknowledges support from the Dr. Manmohan Singh scholarship from St. John's College.